Fractal model of consolidation of weakly aggregated colloidal dispersions

A. A. Potanin* and W. B. Russel
Department of Chemical Engineering, Princeton University, Princeton, New Jersey 08544
(Received 26 October 1995)

A microrheological model for the consolidation of aggregated colloidal dispersion is presented. Interparticle forces are responsible for the formation of the fractal-like network of particles chains. Aggregation is supposed to be weak in that the chains are gradually created and annihilated. In the framework of this model a constitutive equation is proposed which includes linear dependence of the normal stress upon consolidation rate at low stresses and yieldlike behavior as the stress reaches critical value. Our constitutive equation thus generalizes earlier models based on the compressive yield stress concept by taking into account the deformation in the low-compression limit (analog to the Newtonian flow in the low-shear limit). The constitutive equation is employed to calculate numerically concentration profiles of consolidating samples in better agreement with the experimental data for weakly aggregated alumina dispersions.

PACS number(s): 82.70.−y

I. INTRODUCTION

In recent years a number of works have interpreted the viscoelastic properties of aggregating colloids in terms of the mechanics of fractal networks [1–4], assuming that the aggregated structure transmits stress through the chains comprising the elastic backbone. While strongly aggregated chains do not permit the network to flow until the stress reaches the yield point (*shear yield stress*), weakly aggregated chains flow even in the low-stress limit, maintaining an equilibrium between chain creation and annihilation and yielding a *low-shear Newtonian viscosity*. In the latter case the viscoelastic properties of the colloidal network resemble those of polymeric ones, permitting application of the transient network models developed for the latter [5].

All the works cited above treat the shear flow realized in rheological measurements. However, deformation of the network also results from normal stresses, as in a gravitational field or during filtration. Again, one can distinguish strongly aggregating systems which do not consolidate until the normal stress reaches the yield point (*compressive yield stress*), from weakly aggregating ones which undergo compression in the low-stress limit, as characterized by a *low-compression bulk viscosity*. Many workers considered the former case [6–8], but latter has yet to be considered.

In this paper we employ the transient network approach to estimate the bulk viscosity in the low-compression limit. The deformation does not perturb the network significantly if the lifetime of a chain, limited by its thermal breakup, is much shorter than the time required to break it by compression. Equivalently, this holds true if the stress does not exceed some critical value, which we will estimate and still call the compressive yield stress. Our model assumes deformation at constant bulk viscosity up to the yield stress.

In Sec. II we employ the *microscopical* model of the flocculated network [5] to estimate the bulk viscosity and yield stress. Section III presents our numerical calculations of the one-dimensional (1D) consolidation along with analytic results for the small-time limit. As distinct from the analyses in Sec. II, these calculations are *macroscopic* (or phenomenological) requiring no information about the microstructure. However, the microscopic analyses becomes useful in Sec. IV, where we estimate the parameters involved in the constitutive equation to compare the results of our calculations with the experiments of Bergström [9] on consolidation of alumina dispersions. This demonstrates semiquantitative agreement with the experiments for values of network parameters consistent with our model.

II. MICROSCOPIC MODELING: COMPRESSION OF FRACTAL NETWORK

We assume all particles to exist in *chains*, which in turn are combined into a *network* (see Fig. 1). Assuming the frac-

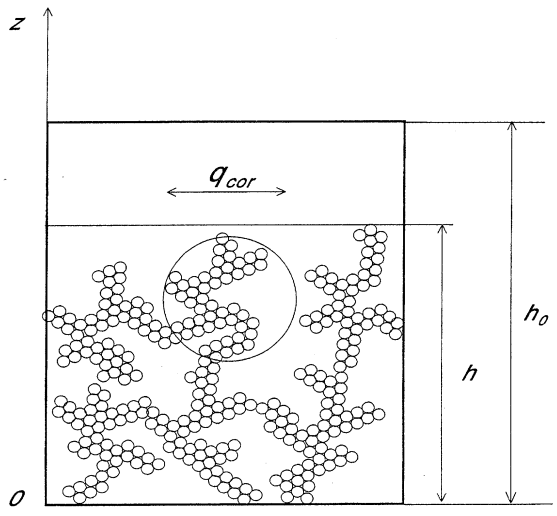

FIG. 1. Schematic of consolidating fractal network with multiply connected chains.

*Present address: Center for Materials for Information Technology (MINT), Bevill research building, University of Alabama, Tuscaloosa, AL 35487-0209.

1063-651X/96/53(4)/3702(8)/$10.00

tal properties of the network and identifying the end-to-end distance of chains, q, with the correlation length of the network, $q_{\rm cor}$, we write (see, e.g., [10])

$$q/a \sim q_{\rm cor}/a \sim \phi^{-1/(3-d_f)}, \tag{1}$$

where ϕ is the volume fraction of solid, d_f is the fractal dimension, a is the particle radius. The number of particles per chain, $N_{\rm ch}$, is related to q via a power law:

$$N_{\rm ch} \sim (q/a)^{d_1}, \tag{2}$$

where d_1 is the chemical dimension (or chemical length exponent), which ranges between 1 (straight chains) and ≈ 1.6 (self-avoiding random walk). Some fraction of the chains is supposed to be *elastically active*, i.e., able to transmit elastic forces which give rise to network stress tensor $\mathbf{T}$. Such chains are modeled as curved elastic rods, which respond to external load as Hookean springs, transmitting the force $\mathbf{f}$ that increases linearly with elongation, Δq,

$$\mathbf{f} = k_e \Delta q \, \frac{\mathbf{q}}{q}, \tag{3}$$

where the force constant [11]

$$k_e \sim k_{e1} (q/a)^{-2-d_1}, \tag{4}$$

decreases with increasing length and k_{e1} characterizes the bending elasticity of a unit section of the chain (see below). Ends of elastically active chains connect to *junctions*, which move affinely.

In Cartesian coordinates with the origin at the bottom and a vertical z axis (see Fig. 1) 1D compression is characterized by the deformation rate $\dot{\gamma}(z) \equiv -du_z/dz$, where $\mathbf{u}$ is the particle velocity averaged over the volume much larger then q^3, but much smaller than the macroscopic volume. In the context of the network model we write the stress tensor $\mathbf{T}$ as

$$\mathbf{T} = n \langle \mathbf{qf} \rangle, \tag{5}$$

where n is the number concentration of elastically active chains and brackets denote volume averaging. Substituting (3) into (5) we write

$$T_{zz} \sim n q_z f_z \sim n_1 k_e q^{-2} \Delta q, \tag{6}$$

where $n_1 \equiv n q^3$ is the number of active chains per correlation volume. Since the chains are compressed, Δq is negative. To estimate its absolute value, we distinguish two mechanisms of chains' breakup: fluctuations and rupture under the compressive force. The former limits the lifetime of the chain, τ, i.e., no chain can live longer than τ whether it is loaded or not. The latter limits a chain's deformation, not permitting $|\Delta q|$ to exceed some critical value, $\Delta q_{\rm rup}$. Hence

$$|\Delta q| \sim \min\{q \tau \dot{\gamma}, \Delta q_{\rm rup}\}. \tag{7}$$

Up to this point we have not specified the mechanisms of chain creation and breakup so that Eqs. (6) and (7) stand as general predictions of the network model. Specifying yet undefined quantities τ, k_e, $\Delta q_{\rm rup}$, and n_1 requires further assumptions, which are considered in detail in [5] with respect to shear deformation. Here we briefly analyze the main results.

One of the simplest estimations of τ proposed by Russel *et al.* [12] on the basis of analysis of doublet breakup reads $\tau \sim \tau_0 \exp(U_c/kT_B)$, where U_c is the magnitude of the minimum of the potential, $\tau_0 = 6\pi\mu a^3/kT_B$ is the characteristic diffusion time of an isolated particle with μ the fluid viscosity, and kT_B is the Boltzmann factor. To improve this estimate let us first point out that the lifetime of a chain decreases as the number of particles in it increases. If the chain is modeled by a singly connected train of particles, its lifetime τ will equal

$$\tau \sim \tau_{\rm single}/N_{\rm ch} \sim \tau_{\rm single} (q/a)^{-d_1} \sim \tau_{\rm single} \phi^{d_1/(3-d_f)}, \tag{8}$$

where $\tau_{\rm single}$ is the characteristic time of a single particle to break a bond with one of its neighbors. For a singly connected chain it is easy to show that $\tau_{\rm single}$ differs from τ_0 only by a factor which is rather close to 1. However, in the system of spherical particles with purely central interactions, which we consider here, singly connected chains are elastically active only when straight, while any contorted chain is inactive since the particles will adjust freely.

A more realistic model of colloidal chains implies the chains to be *multiply connected*, i.e., to consist of a bundle of singly connected chains (see Fig. 1). The illustrations of multiply connected chains in 2D are provided by numerical simulations [13] and experimental data [14]. Such a chain may be elastically active even if the interaction of particles is purely central. However, one singly connected point suffices to deactivate the entire chain due to free rotation of particles or sections of the chain in this point. Hence, $\tau_{\rm single}$ in (8) should be understood as the characteristic time of such a deactivation, while $N_{\rm ch}$ should be identified with the number of particles in the chain which can cause such deactivation. We will assume that $N_{\rm ch}$ is still described by Eq. (2). To estimate $\tau_{\rm single}$ we consider one of these particles moving along the trajectory which permits it to pass over the lowest potential barrier. This trajectory is achieved if this particle "rolls" over two of its neighbors to reach a new stable position. The minimum number of bonds to be broken is z and the potential barrier is zU_c, where U_c is the two-particle bond energy. In [5] the reaction rate theory was employed to obtain

$$\tau_{\rm single} \sim \frac{kT_B \delta}{k_0^{1/2} U_c a} \, \tau_0 \, \exp[zU_c/kT_B], \tag{9}$$

where δ is the gap width between aggregated particles.

Two other parameters, k_{e1} and $\Delta q_{\rm rup}$, characterize the response of the chain to external load. As noted above, k_{e1} in (4) represents the bending elasticity of a unit section of a chain. Since we assumed that the elastic response of chains originates from their multiply connected structure, we identify k_{e1} with the force constant of a doublet:

$$k_{e1} \equiv k_0 U_c / \delta^2, \tag{10}$$

where k_0 is dimensionless curvature of the potential well.

For $\Delta q_{\rm rup}$ we employ the estimate

$$\Delta q_{\rm rup} \sim k_0^{-1/2} \delta (q/a)^{1+d_1}, \tag{11}$$

which was derived in [5] assuming the chain to break if stored elastic energy per bond exceeds U_c.

Finally, substituting (7)–(11) into (6), we find a simple constitutive equation:

$$-T_{zz} = \min\left\{ -\eta_v(\phi) \frac{\partial u_z}{\partial z}, \sigma_y(\phi) \right\}, \tag{12}$$

where

$$\eta_v \sim \mu k_0^{1/2} n_1 \frac{a}{\delta} e^{zU_c/kT} \phi^{\gamma} \tag{13}$$

is the bulk viscosity and

$$\sigma_y \sim k_0^{1/2} n_1 \frac{U_c}{a^2 \delta} \phi^{\gamma_y} \tag{14}$$

is the compressive yield stress,

$$\gamma \equiv (3+2d_1)/(3-d_f), \quad \gamma_y \equiv 3/(3-d_f).$$

Now the only undefined parameter in (12)–(14) is the number of active chains per junction, n_1. Obviously, n_1 should be an increasing function of volume fraction. In the extreme case $\phi \to \phi_m$, where ϕ_m is the maximum attainable volume fraction (below we identify ϕ_m to the volume fraction at random close packing of spheres, $\phi_m = 0.64$), the network transforms from the fractal to a compact one, which can be interpreted as divergence of $n_1(\phi)$. Assuming the simplest form of this divergence we write

$$n_1 \sim \left(1 - \frac{\phi}{\phi_m}\right)^{-\kappa}, \tag{15}$$

where κ is a parameter to be specified below. Of course, (15) should be considered as a phenomenological assumption introduced in order to apply the fractal model even beyond its actual applicability, i.e., at high ϕ, as relevant to the latter stages of consolidation. Note that a similar divergent factor with $\kappa = 1$ was introduced by Bergström [9] yielding $\sigma_y \propto \phi^{\gamma_y}/[1-(\phi/\phi_m)]$. More generally, κ and ϕ_m can be considered as adjustable parameters.

III. MACROSCOPIC MODELING: NETWORK CONSOLIDATION IN GRAVITY FIELD

A. General formulation

The pioneering work on modeling of consolidation was done by Buscall and White [6] and followed by Auzarais *et al.* [7]. Here we modify these works as discussed below.

We start from the general force balance equation

$$\nabla \mathbf{T} + \mathbf{f} = \mathbf{0}, \tag{16}$$

where the body force $\mathbf{f}$ includes gravity and viscous drag as

$$\mathbf{f} = \Delta\rho\phi\mathbf{g}\left(1 + r(\phi)\frac{\mathbf{u}_{\rm med} - \mathbf{u}}{v_0}\right), \tag{17}$$

$\Delta\rho$ is the difference in mass density of the solid and liquid phase, $\mathbf{u}_{\rm med}$ is the medium velocity, and $\mathbf{g}$ is the gravity acceleration. The collective friction $r(\phi)$ accounts for the effect of hydrodynamic interactions on the sedimentation velocity, $v(\phi)$, which corresponds to the movement of the infinite structure through the liquid without consolidation as $r(\phi) = v_0(1-\phi)/v(\phi)$ with $v_0 \equiv 2\Delta\rho g a^2/9\mu$. Conservation of mass implies $\mathbf{u} - \mathbf{u}_{\rm med} = \mathbf{u}/(1-\phi)$. For 1D consolidation (16) and (17) determine the network velocity:

$$u_z = -v(\phi)\left(1 - \frac{\partial T_{zz}/\partial z}{\Delta\rho g \phi}\right) \tag{18}$$

for substitution into the continuity equation

$$\frac{\partial \phi}{\partial t} + \frac{\partial(\phi u_z)}{\partial z} = 0. \tag{19}$$

Substituting constitutive equation (12) into (18) and converting (18) and (19) to dimensionless variables yields

$$U = V(\phi)\left[1 + \frac{1}{\phi}\frac{\partial}{\partial Z}\min\left\{\sigma\Sigma(\phi), \eta\mathscr{H}(\phi)\frac{\partial U}{\partial Z}\right\}\right], \tag{20}$$

$$\frac{\partial \phi}{\partial T} = \frac{\partial}{\partial Z}(\phi U), \tag{21}$$

where

$$Z \equiv z/h_0, \quad T \equiv tv(\phi_0)/h_0, \quad U \equiv -u_z/v(\phi_0),$$

$$V(\phi) \equiv v(\phi)/v(\phi_0),$$

$$\Sigma(\phi) \equiv \sigma_y(\phi)/\sigma_y(\phi_0), \quad \mathscr{H}(\phi) \equiv \eta_v(\phi)/\eta_v(\phi_0),$$

$$\sigma \equiv \frac{\sigma_y(\phi_0)}{\Delta\rho g h_0}, \quad \eta \equiv \frac{\eta_v(\phi_0)v(\phi_0)}{\Delta\rho g h_0^2},$$

h_0 is the height of a sample in which solid phase is distributed with volume fraction ϕ_0 at time $t=0$ (see Fig. 1). Thus, the network initially fills the sample, while during the consolidation the particles are redistributed so that the boundary between the network and pure liquid at $z=h$ goes down, i.e., $H \equiv h/h_0$ is a decreasing function of T. Hence, initial conditions are

$$\phi(Z, T=0) = \phi_0, \quad H(T=0) = 1, \tag{22}$$

while boundary conditions specify no flux at the bottom and zero stress at the top:

$$U(Z=0, T) = 0, \tag{23a}$$

$$\frac{\partial U(Z=H, T)}{\partial Z} = 0. \tag{23b}$$

Rewriting (20) separately in the upper ($Z > Z_c$) and lower ($Z < Z_c$) zones, with Z_c the interface between them, yields:

$$U = V(\phi)\left\{1 + \frac{\eta}{\phi}\frac{\partial}{\partial Z}\mathscr{H}(\phi)\frac{\partial U}{\partial Z}\right\}, \quad Z > Z_c, \tag{24}$$

$$U=V(\phi)\left\{1+\frac{\sigma}{\phi}\frac{\partial}{\partial Z}\Sigma(\phi)\right\}, \quad Z<Z_c. \tag{25}$$

The latter equation is conveniently rewritten as

$$\frac{\partial\phi}{\partial Z}=\frac{\phi}{D(\phi)}[U-V(\phi)], \tag{26}$$

where

$$D(\phi)\equiv\sigma V(\phi)\frac{d\Sigma(\phi)}{d\phi}. \tag{27}$$

Equations (24) and (26) should be solved together with (22) and (23) and their solutions joined at $Z=Z_c$ such that T_{zz}, U, and ϕ are continuous:

$$\eta\mathscr{H}(\phi)\left.\frac{\partial U}{\partial Z}\right|_{Z=Z_c+0}=\sigma\Sigma(\phi)|_{Z=Z_c-0}, \tag{28}$$

$$U|_{Z=Z_c+0}=U|_{Z=Z_c-0}, \tag{29}$$

$$\phi|_{Z=Z_c+0}=\phi|_{Z=Z_c-0}. \tag{30}$$

We refer to the solution of the general equations (24), (26), and (28)–(30) as the *combined* model as opposed to the *pure-Newtonian* ($\sigma\to\infty$) and *pure-yield* ($\eta\to\infty$) cases.

B. Short-time analysis

An analytic solution exists in $T\to 0$ limit. Setting $\phi=\phi_0$ in (24) we find

$$U(Z>Z_c,T\to 0)=1+C_1\{\exp(Z/\sqrt{\eta})+\exp[(2-Z)/\sqrt{\sigma}]\}, \tag{31}$$

and

$$\phi(Z>Z_c,T\to 0)=\phi_0+0(T), \tag{32}$$

where C_1 is undefined. At $Z<Z_c$ we employ (20) to rewrite (26) as

$$\frac{\partial\phi}{\partial T}=D(\phi)\frac{\partial^2\phi}{\partial Z^2}+\frac{dD(\phi)}{d\phi}\left(\frac{\partial\phi}{\partial Z}\right)^2+\left(V-\phi\frac{dV(\phi)}{d\phi}\right)\frac{\partial\phi}{\partial Z}. \tag{33}$$

where $D(\phi)$ is defined in (27). As shown by Howells *et al.* [15] the last two terms in the rhs are negligible as $T\to 0$, reducing (33) to the unsteady diffusion equation with solution

$$\phi(Z<Z_c,T\to 0)=1-\sqrt{2T/D(1)}\,\xi+C_2\sqrt{T}\left(\exp(-\xi^2/2)+\xi\int_0^{\xi}\exp(-\xi^2/2)d\xi\right), \tag{34}$$

$$U(Z<Z_c,T\to 0)=C_2\sqrt{D(\phi_0)/2}\int_0^{\xi}\exp(-\xi^2/2)d\xi, \tag{35}$$

where $\xi\equiv Z/\sqrt{2TD(\phi_0)}$ and C_2 is another yet undefined coefficient. Substituting (31), (32), (34) and (35) into (29) and (30) we find

$$C_1=\frac{I-1}{\exp(Z_c/\sqrt{\eta})+\exp[(2-Z_c)/\sqrt{\eta}]},$$

$$C_2=\frac{\xi_c\sqrt{2/D(\phi_0)}}{\exp(-\xi_c^2/2)+\xi_c\int_0^{\xi_c}\exp(-\xi^2/2)d\xi}, \tag{36}$$

where

$$I\equiv\frac{\xi_c\int_0^{\xi_c}\exp(-\xi^2/2)d\xi}{\exp(-\xi_c^2/2)+\xi_c\int_0^{\xi_c}\exp(-\xi^2/2)d\xi}. \tag{37}$$

Now we make use of (28) to find Z_c as a solution of the following equation:

$$(1-I)\sqrt{\eta}\tanh\frac{1-Z_c}{\sqrt{\eta}}=\sigma. \tag{38}$$

Hence the two-zone solution presented above develops at the bottom only at

$$\sqrt{\eta}\tanh\frac{1}{\sqrt{\eta}}>\sigma. \tag{39}$$

In the high-viscosity limit, $\eta\to\infty$, pure-yield flow is realized, in which case (39) reduces to the yield condition $\sigma<1$ stated by Buscall *et al.* [6]. At lower viscosity yield flow has to compete with viscous flow. If σ becomes higher than the lhs of (39), the viscous flow completely dominates. As η decreases the lhs of (39) decreases, thus reducing the range of σ in which yield flow develops [note that (39) reduces to $\sqrt{\eta}>\sigma$ at $\eta\to 0$].

If (39) is not satisfied, U is given by (31), which takes the form

$$U(Z,T\to 0)=1-\frac{\exp[Z/\sqrt{\eta}]+\exp[(2-Z)/\sqrt{\eta}]}{1+\exp[2/\sqrt{\eta}]}, \tag{40}$$

while ϕ is found through time integration of (21) with (40)

$$\phi(Z,T\to 0)=1+\frac{T}{\sqrt{\eta}}\frac{\exp[(2-Z)/\sqrt{\eta}]-\exp[Z/\sqrt{\eta}]}{1+\exp[2/\sqrt{\eta}]}. \tag{41}$$

As expected, the maximum value of the viscous stress, $\eta(\phi)\partial u_z/\partial z$, indeed remains lower than σ as long as the inequality opposite to (39) is satisfied.

In conclusion of our short-time analysis, let us represent the initial rate of change of the sediment height:

$$U_0\equiv U(Z\to 1,T\to 0)=1-\sigma f_{\text{sed}}(\eta), \tag{42}$$

where

$$f_{\rm sed}(\eta)\equiv\min\left\{\frac{1}{\sigma},\ \frac{1}{\sqrt{\eta}\tanh\dfrac{1}{\sqrt{\eta}}}\right\}\frac{2\exp(1/\sqrt{\eta})}{1+\exp(2/\sqrt{\eta})}. \tag{43}$$

Recall that in pure yield case $\eta\to\infty$ with $\sigma<1$ [i.e., if (39) is satisfied] (42) reduces to $f_{\rm sed}=1$, as first obtained by Buscall *et al.* [6].

C. Numerical procedures

The basis of our calculations is the well known Runge-Kutta shooting method (RKSM). Let us first consider limiting cases to which one-zone solutions apply.

The *pure Newtonian case* is realized if

$$\eta\mathscr{H}(\phi)\frac{\partial U}{\partial Z}<\sigma\Sigma(\phi) \tag{44}$$

is satisfied at every Z and T. In this case Z_c is set to zero and (24) is integrated with (23) via RKSM to determine U at given T. This also gives us dH/dT as $-U(Z=H)$. With these we calculate ϕ through (21), which is subsequently used in the next step, $T+\Delta T$, etc.

The *pure yield case* corresponds to the limit $\eta\to\infty$. In this case the problem is easy to solve since $\phi(Z_c\le Z\le H,T)=\phi_0$ and $U_c\equiv U(Z_c,T)$ is related to Z_c through direct integration of (18) from Z_c to H with $\phi=\phi_0$, $T_{zz}(Z=H)=0$, and $T_{zz}(Z=Z_c)=-\sigma_y(\phi=\phi_0)$. This gives a closure as $U_c=1+[\eta/(H-Z_c)]$. Starting from the known short-time solution (34) and (35) (which are easily seen to hold true for pure yield as well) we calculate ϕ and U at T through RKSM with $\partial\phi/\partial T$ estimated as $[\phi(Z,T)-\phi(Z,T-\Delta T)]/\Delta T$. This algorithm is described in detail by Howells *et al.* [15].

Our general algorithm is shown schematically in Table I. As noted above, the two-zone consolidation flow develops if (39) is satisfied. In this case our algorithm calculates ϕ and U in both zones as shown in Table II. This procedure combines an algorithm of Howells *et al.* [15] for the lower zone with the RKSM algorithm for calculating U [ϕ is subsequently found from (21)] in the upper zone. The latter is similar to the one for the Newtonian case, but with floating lower bound Z_c which is found from joining these two solutions.

Now let us discuss in some detail our algorithm for the two-zone solution (Table II). The basic idea is that at every time step we iteratively adjust the bottom, $\phi_b\equiv\phi(Z=0,T)$, and interface (between viscous and yield zones), $\phi_c\equiv\phi(Z=Z_c,T)$, concentrations to satisfy boundary conditions (23) and (28–30). This is accomplished by guessing, ϕ_b^* and ϕ_c^* for ϕ_b and ϕ_c, respectively, and subsequently shooting via the RKSM algorithm. We start with a guess, ϕ_c^*, for the interface concentration. For the given ϕ_c^* we employ the iterative procedure to determine the bottom concentration (dashed-line block in Table II). At the Nth iteration the procedure starts by making a guess, $\phi_b^*(N)$, and calculating ϕ and U in both zones satisfying boundary conditions (28) and (29), but instead of (30) we satisfy the condition $\phi|_{Z=Z_c-0}=\phi_c^*$. The condition (23b) is also impossible to satisfy unless we properly chose ϕ_b^*. Thus, we keep on shooting trying to adjust ϕ_b^* iteratively to minimize the absolute value of the lhs of (23b). The procedure is completed when subsequent iterations yield ϕ_b^* within the tolerance interval. After that we check whether our choice of ϕ_c^* was close enough to the value $\phi_c^{**}\equiv\phi|_{Z=Z_c+0}$ yielded

TABLE I.

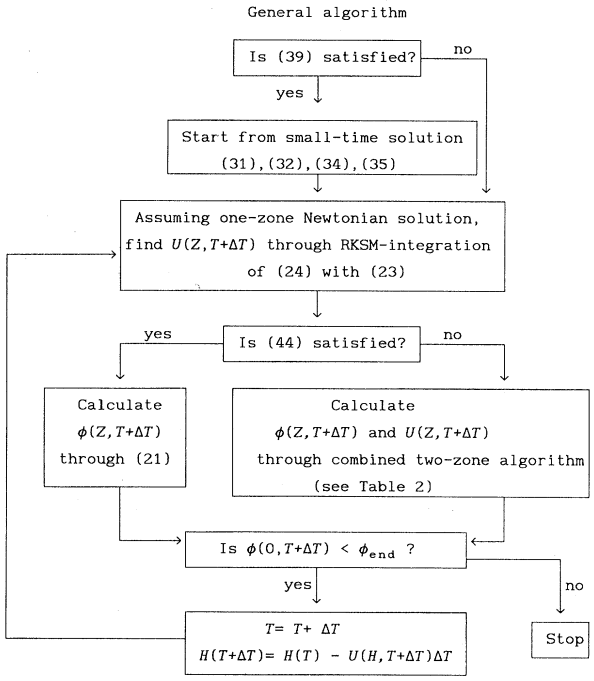

TABLE II.

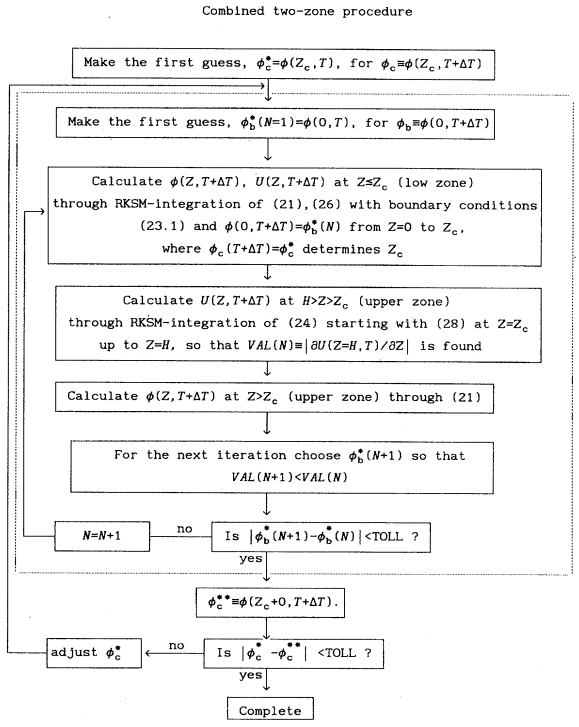

by shooting. We iteratively adjust ϕ_b^* until ϕ_c^* converges to ϕ_c^{**}.

At each step our algorithm checks whether (44) is satisfied, i.e., that the solution can be obtained in the pure Newtonian form. If this is impossible, the two-zone solution is obtained as described above. However, as the flow slows down, the two-zone flow always undergoes a transition to the pure-Newtonian pattern with ϕ tending asymptotically to ϕ_m. In practice one has to stop calculations at some point, say as ϕ_b reaches ϕ_{end}.

IV. RESULTS

A. General calculations

To perform the calculations we need to specify the function $v(\phi)$, which enters into our equations. To this end we employ a modified Brinkman equation

$$v(\phi)=Cv_0\frac{(2-3\phi)^2}{3\phi+4+3(8\phi-3\phi^2)^{1/2}}, \tag{45}$$

where C accounts for the fact that the particles are arranged in chains. In such an arrangement even in the limit $\phi\to 0$, v is higher that v_0 due to screening of the hydrodynamic resistance, i.e., $C>1$ being an increasing function of the coordination number. The actual value of C is not essential as long as we present our results in dimensionless form, since it only rescales the real time values. To fit the experimental data in the next subsection we consider C an adjustable parameter.

The exponents in the constitutive equation (12) were defined as

$$\gamma=5, \quad \gamma_y=3, \quad \kappa=1. \tag{46}$$

Note that the first two are in accordance with our fractal model at $d_f=2$ and $d_1=1$. The last one sets the divergence in η_v and σ_y and is identical to the one used by Bergström [9].

A pure yield solution ($\eta\to\infty$) is shown in Fig. 2. In this case the concentration profile tends asymptotically to equilibrium, $\phi(Z,T)\to\phi_{\text{eq}}(Z)$, such that

$$1+\sigma\frac{d\Sigma(\phi)}{d\phi}\frac{d\ \ln\ \phi_{\text{eq}}}{dZ}=0$$

at $Z<Z_c$ (yield consolidation),

$\phi_{\text{eq}}=1$ at $H<Z<Z_c$ (no consolidation).

As σ decreases, consolidation spreads deeper into the sample.

For finite η the profile develops as demonstrated in Fig. 3 with zones coexisting until the lower one disappears at $T=T_c$. After that Newtonian consolidation proceeds up to close packing (asymptotically) as opposed to the pure yield solution, see Fig. 4. For fixed η the yield zone quickly widens as σ is decreased, see Fig. 5, but always disappears at $T=T_c$, making the late-stage consolidation insensitive to σ.

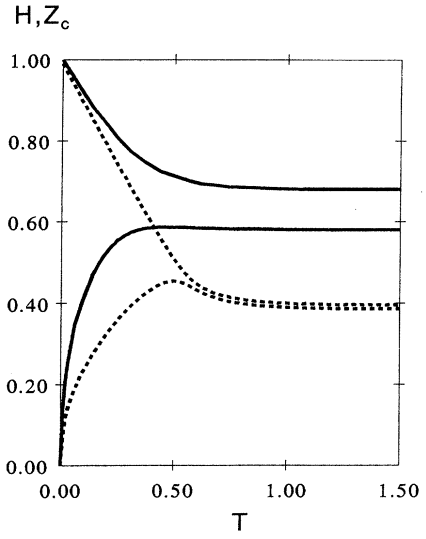

FIG. 2. Dimensionless heights of consolidating sample, H (upper curves), and the lower zone, Z_c (lower curves), plotted vs dimensionless time T for pure yield model at $\sigma=0.015$ (solid) and $\sigma=0.0015$ (dashed), $\phi_0=0.15$.

B. Comparison with the experiments

Now we will compare our calculations with the experimental data of Bergström [9]. We set

$$a=0.2\ \mu\text{m}, \quad \Delta\rho=3100\ \text{kg/m}^3, \quad \mu=2.6\ \text{mPa s},$$

$$h_0=0.2\ \text{m}, \quad \phi_0=0.15,$$

$$U_c=11kT_B, \quad \delta=5\ \text{nm}, \quad k_0\sim 100, \tag{47}$$

which corresponds to his dispersion of alumina particles stabilized by the adsorbed layer of oleic acid.

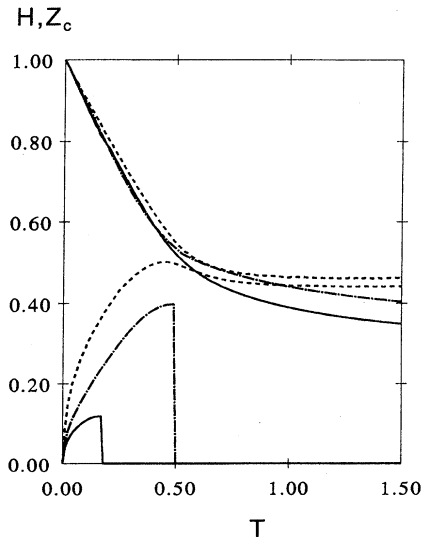

FIG. 3. Same as in Fig. 2 for two-zone calculations (solid curves) at $\sigma=0.003$ for pure yield model $\eta=\infty$ (---), and combined model at $\eta=0.0015$ (–·–·–) and $\eta=0.000\,45$ (—).

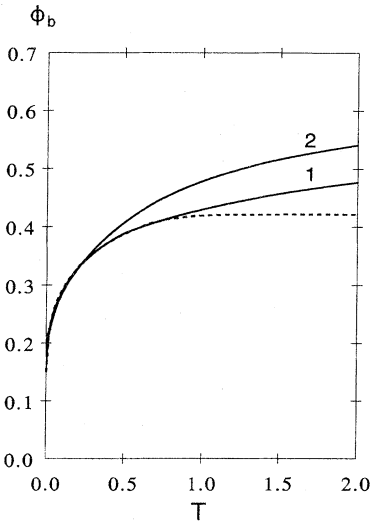

FIG. 4. Dimensionless bottom volume fraction is plotted vs T at $\sigma=0.003$ for pure yield model $\eta=\infty$ (dashed curve), and combined model at $\eta=0.0015(1)$ and $\eta=0.000\,45(2)$.

Let us first consider pure yield calculations. With (47) we find from (14) $\sigma_y(\phi_0)\sim 10$ Pa, i.e., $\sigma=1.6\times10^{-3}$. Fitting the experimental data with the only adjustable parameter, C, we find the best agreement at $C=1.5$. The results are presented in Fig. 6. One can see that this approach quantitatively describes the main features of the consolidation process, but fails in two predictions: (i) that consolidation occurs only at the bottom of the sample, rather than throughout the sample; (ii) that the process stops with the equilibrium profile, $\phi_{eq}(Z)$, rather than proceeding further up to $\phi\rightarrow\phi_m$, although very slowly.

In Fig. 7 we compare the calculations for the pure Newtonian model with the same experimental data. One can see

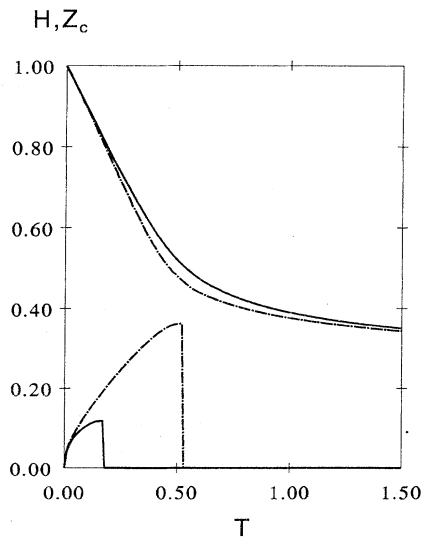

FIG. 5. Same as in Fig. 3 at fixed $\eta=0.000\,45$ for $\sigma=0.003$ (solid) and $\sigma=0.0015$ (dashed).

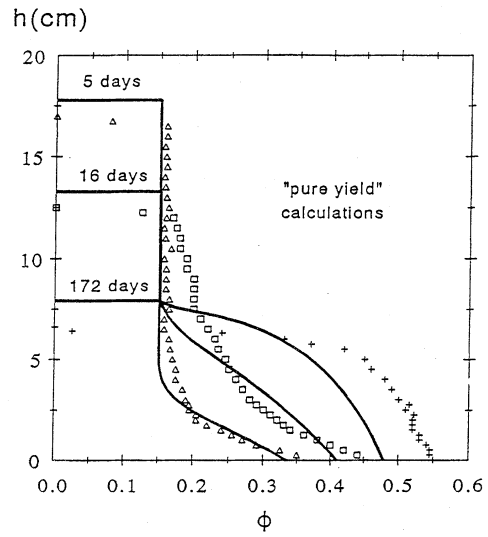

FIG. 6. Concentration profile in consolidating sample at different moments of time. Calculations for pure yield model ($\eta=\infty$) at $\sigma=0.0015$, $\gamma_y=3$, $C=1.5$.

that now the consolidation occurs throughout the sample, rather than only at the bottom, and the concentration profile in the latest stages of consolidation is very close to the experimental one. However, the calculation underestimates the volume fraction at the bottom, which can be attributed to the fact that the yield zone emerges there. In our calculations we set $\eta=4.5\times10^{-4}$, which corresponds to calculations with (13) and (47) at $z=2.05$ [bulk viscosity in the initial sample is $\eta_b(\phi_0)=4.3\times10^9\ \mu$].

The results of the two-zone (combined) calculations are presented in Fig. 8, which turn out to agree better with the

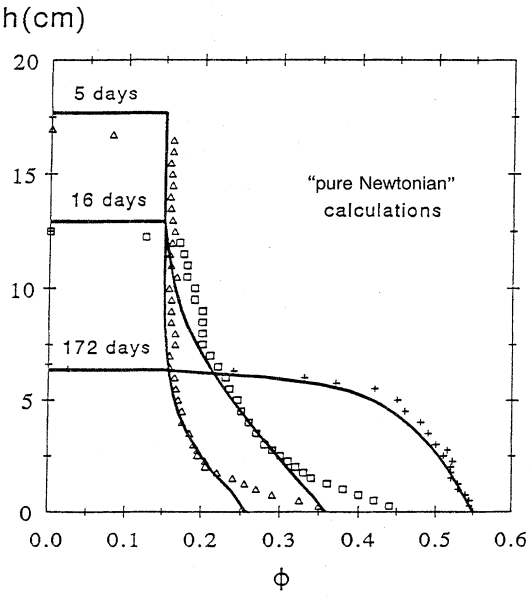

FIG. 7. Same as in Fig. 6 for pure Newtonian model ($\sigma=\infty$) at $\eta=0.000\,45$, $\gamma=5$, $C=1.5$.

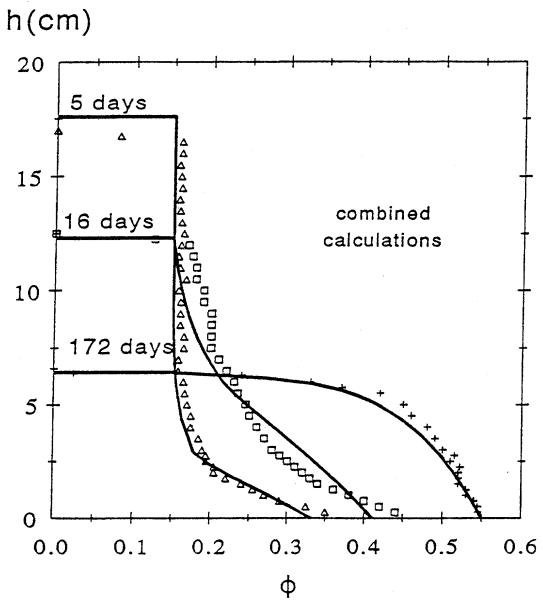

FIG. 8. Same as in Figs. 6 and 7 for the two-zone (combined) calculations with the same parameters.

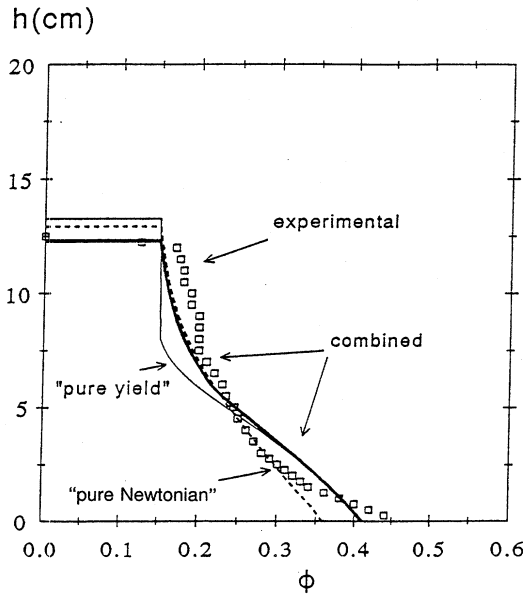

FIG. 9. Curves from Figs. 6–8 at $t=16$ days are plotted together.

experiments than one-zone calculations considered above. This is also demonstrated in Fig. 9, where we have plotted the profiles calculated via all three algorithm in one plot. One can see that the two-zone calculations predict faster rate of consolidation everywhere in the sample than any of the one-zone algorithms.

V. CONCLUSIONS

We have presented a microrheological model for consolidation of aggregated dispersions under gravity. The model assumes a transient fractal network to be responsible for normal stresses providing a constitutive equation with constant bulk viscosity at low stresses and yieldlike behavior as the stress reaches critical value. Thus, our model generalizes an earlier one based on the compressive yield stress alone by accounting for deformation at lower stresses, which dominates at the latest stages of consolidation and permits the volume concentration to approach close packing asymptotically. We employed our constitutive equation to calculate numerically the consolidation of a particular fractal network and found better agreement with the experimental data for weakly aggregated alumina dispersions than with the compressive yield stress model.

ACKNOWLEDGMENTS

One of the authors (A.A.P.) acknowledges the financial support of the International Fine particle Research Institute and the partial support of the International Science Foundation (Grant No. NCY000).

[1] W. B. Russel, Powder Technol. **51**, 15 (1987).
[2] L. C. G. Bremer, B. H. Bijsterbosch, R. Schrijevens, T. van Vliet, and P. Walstra, Colloids Surf. **51**, 159 (1990).
[3] R. Wessel and R. C. Bal, Phys. Rev. A **46**, 3008 (1992).
[4] R. De Rooij, A. A. Potanin, D. van den Ende, and J. Mellema, J. Chem. Phys. **99**, 9213 (1993).
[5] A. A. Potanin, R. De Rooij, D. van den Ende, and J. Mellema, J. Chem. Phys. **102**, 5845 (1995).
[6] R. Buscall and L. R. White, J. Chem. Soc. Faraday Trans. 1, **83**, 873 (1987).
[7] F. M. Auzerais, R. Jackson, and W. B. Russel, J. Fluid Mech. **195**, 437 (1988).
[8] K. Landman and W. B. Russel, Phys. Fluid A **5**, 550 (1993).
[9] L. Bergström, J. Chem. Soc. Faraday Trans. **88**, 3201 (1992).
[10] R. Jullien and R. Bottet, *Aggregation and Fractal Aggregates* (World Scientific, Singapore, 1987).
[11] Y. Kantor and I. Webman, Phys. Rev. Lett. **52**, 1891 (1984).
[12] W. B. Russel, D. A. Saville, and W. R. Schowalter, *Colloidal Dispersions* (Cambridge University Press, Cambridge, U.K., 1988).
[13] A. H. L. West, J. R. Melrose, and R. C. Ball, Phys. Rev. E **49**, 4237 (1994).
[14] A. T. Skjeltorp, Phys. Rev. Lett. **51**, 2306 (1987).
[15] I. Howells, K. Landman, A. Panjkov, C. Sirakoff, and L. R. White, Appl. Math. Model. **14**, 77 (1990).